

A study of square-well statistical associating fluid theory approximations

Hertanto Adidharma, Maciej Radosz *

Department of Chemical Engineering and Macromolecular Studies Group, Louisiana State University, Baton Rouge, LA 70803-7303, USA

Received 4 December 1998; accepted 3 March 1999

Abstract

Six square-well (SW) statistical associating fluid theory (SAFT) models, fitted to the experimental saturated liquid volume and saturated vapor pressure for pure *n*-alkanes, are analyzed for predicting the coexisting densities, second virial coefficients, and binary phase equilibria. The models that result in low values of the segment energy and weak molecular weight dependence of the parameters are found to be more accurate for real fluids. The inclusion of the dimer structure in the SW chain term seems to produce no significant benefit for representing real substances. © 1999 Elsevier Science B.V. All rights reserved.

Keywords: Equation of state; Perturbation theory; Square-well SAFT; Dimer reference; Vapor pressure; Liquid density; Second virial coefficient; Alkanes

1. Introduction

One of the approaches to developing equations of state for chain fluids is on the basis of the thermodynamic perturbation theory of the first order (TPT1) of Wertheim [1–4]. A generic approach to implementing TPT1 to real fluids, referred to as the statistical associating fluid theory (SAFT), can be found in Ref. [5].

The SAFT equations of state have the following terms: a *segment term* that accounts for the non-ideality of the reference fluid of non-bonded chain segments (monomers), a *chain term* that accounts for covalent bonding, and an *association term* that accounts for hydrogen bonding that leads to association. There may also be an optional term that accounts for polarity. The chain and association terms are estimated on the basis of the pair correlation function of the reference (non-bonded segment) fluid alone.

* Corresponding author. Tel.: +1-225-388-1750; fax: +1-225-388-1750; e-mail: radosz@che.lsu.edu

For example, Huang and Radosz [6] developed a SAFT equation of state on the basis of an argon equation of state (the so-called BACK equation of state) for the segment term and a hard-sphere pair-correlation function for the chain term. The Huang–Radosz version of SAFT has parameters that are well-behaved and hence, relatively easy to estimate for large molecules. Furthermore, this version has been extended to heterobonded chains by Banaszak et al. [7]. That extension, referred to as copolymer SAFT, explicitly accounts for variable polyolefin microstructure due to the variability in comonomer incorporation.

The challenge is to make SAFT more predictive and to make the parameters even easier to estimate. Different approaches to improving SAFT fall into two categories: one approach utilizes the Lennard–Jones (LJ) fluid as the reference, as it is described, e.g., by Banaszak et al. [8,9] and in the references therein. Another approach utilizes the square-well (SW) fluid as the reference, as it is described, e.g., by Banaszak et al. [10] and in the references therein. In both approaches, we need two crucial expressions for the reference non-bonded fluid: an equation of state and a radial distribution function, both valid over the whole temperature, density, energy, and diameter ranges.

The focus of this work is on the SW-based SAFT. We build on theoretical concepts and data reported for SW fluids in Refs. [11–14].

The purpose of this work is to understand how different approaches to approximating the Helmholtz energy and the radial distribution function of the SW fluid affect the SAFT equations of state they underpin. Specifically, we look at the accuracy of correlating and predicting pure-alkane properties and mixed-alkane equilibria, and at the behavior of pure-component parameters. This is a narrow analysis, only from the SAFT point of view, without an attempt to evaluate these approximations in general or to formulate a new equation of state.

2. Generic SAFT model

The generic SAFT model is based on Wertheim’s TPT1. The constant volume residual Helmholtz energy per mole a^{res} , the residual Helmholtz energy for short, can be defined as:

$$a^{\text{res}}(T, V, N) \equiv a(T, V, N) - a^{\text{ideal}}(T, V, N), \quad (1)$$

where $a(T, V, N)$ is the Helmholtz energy per mole of molecules of the real fluid and $a^{\text{ideal}}(T, V, N)$ is the Helmholtz energy per mole of the ideal gas at the same temperature and density. Dropping the (T, V, N) specification in our notation, the residual Helmholtz energy consists of three terms [5]:

$$a^{\text{res}} = a^{\text{seg}} + a^{\text{chain}} + a^{\text{assoc}}, \quad (2)$$

where a^{seg} is the Helmholtz energy due to segment–segment within the reference system, a^{chain} is the incremental Helmholtz energy due to chain formation, and a^{assoc} is the incremental Helmholtz energy due to association, e.g., due to hydrogen bonding. The role of the unperturbed (reference) system can be assigned to any fluid having known Helmholtz energy and radial distribution function.

From Eq. (2), the molar residual Helmholtz energy for non-associating alkane fluids studied in this work is given by:

$$a^{\text{res}} = a^{\text{seg}} + a^{\text{chain}}. \quad (3)$$

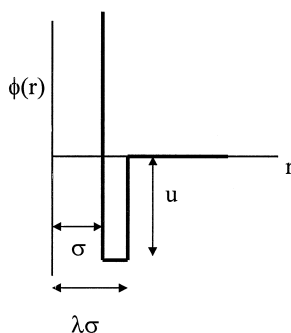


Fig. 1. The SW potential model.

The segment contribution can be expressed in terms of the Helmholtz energy per segment, a_o^{seg} , i.e.,

$$\frac{a^{\text{seg}}}{RT} = \tilde{a}^{\text{seg}} = m\tilde{a}_o^{\text{seg}}, \quad (4)$$

where m is the number of segments per molecule. Tilde (\sim) used in this work means a dimensionless form of a variable. The chain contribution is related to the radial distribution function of the reference fluid at contact $g^{\text{ref}}(\sigma)$ as follows [13]:

$$\tilde{a}^{\text{chain}} = -(m-1)[\ln g^{\text{ref}}(\sigma) - \ln g_0^{\text{ref}}(\sigma)], \quad (5)$$

where $g_0^{\text{ref}}(\sigma)$ is the radial distribution function of the reference monomer fluid at contact and at zero density.

3. Perturbation theory for SW fluid

The SW fluid has a steep repulsion at short distances and a short-ranged attraction at intermediate distances. Its potential model is characterized by three parameters, i.e., the hard-sphere diameter (σ), the well depth (u) and the reduced range of the potential well (λ), as shown in Fig. 1.

The potential energy for a pair of SW segments separated by a distance r is given by:

$$\phi(r) = \phi^{\text{hs}}(r, \sigma) - \phi_1(r, \lambda), \quad (6)$$

where ϕ^{hs} is the unperturbed potential, i.e., the hard-sphere potential, given by:

$$\phi^{\text{hs}}(r, \sigma) = \begin{cases} \infty & \text{if } r < \sigma, \\ 0 & \text{if } r > \sigma, \end{cases} \quad (7)$$

and ϕ_1 is the perturbation given by:

$$\phi_1(r, \lambda) = \begin{cases} 0 & r < \sigma, \\ u & \sigma < r < \lambda\sigma, \\ 0 & r > \lambda\sigma. \end{cases} \quad (8)$$

The segment Helmholtz energy a_o^{seg} in Eq. (4) and the radial distribution function in Eq. (5) are estimated from the SW potential on the basis of perturbation theory for dense fluids developed by Barker and Henderson [17]. The segment term is then expressed as:

$$\tilde{a}_o^{\text{SW}} = \tilde{a}_o^{\text{hs}} + \tilde{a}_o^{\text{disp}}, \quad (9)$$

where \tilde{a}_o^{hs} is the hard-sphere Helmholtz energy per segment, calculated from the Carnahan–Starling (CS) [16] equation, and $\tilde{a}_o^{\text{disp}}$ is the dispersion term per segment given by (up to the second order):

$$\tilde{a}_o^{\text{disp}} = \frac{1}{T^*} \tilde{a}_1 + \frac{1}{(T^*)^2} \tilde{a}_2. \quad (10)$$

Here, T^* is the reduced temperature defined by kT/u , k is the Boltzmann constant, T is the temperature, \tilde{a}_1 is the first perturbation term and \tilde{a}_2 is the second perturbation term. For our purposes, it is convenient to rewrite Eq. (10) as follows:

$$\tilde{a}_o^{\text{disp}} = \beta a_1 + \beta^2 a_2, \quad (11)$$

where β is $1/kT$, a_1 and a_2 are the first two perturbation terms associated with the attractive energy u , given by McQuarrie [15]:

$$a_1 = u\tilde{a}_1 = -\frac{\rho_s}{2} \int \phi_1 g^{\text{hs}}(r) 4\pi r^2 dr, \quad (12)$$

$$a_2 = u^2 \tilde{a}_2 = -\frac{\rho_s}{4} \int (\phi_1)^2 kT \frac{\partial(\rho_s g^{\text{hs}}(r))}{\partial P^{\text{hs}}} 4\pi r^2 dr. \quad (13)$$

Here, ρ_s is the number density, $g^{\text{hs}}(r)$ is the hard-sphere radial distribution function at distance r , and P^{hs} is the pressure of hard-sphere fluid. The first perturbation term a_1 corresponds to the average of the potential energy calculated with the hard-sphere structure. The second perturbation term a_2 , so-called local-compressibility approximation, describes the fluctuation of the attractive energy. Eq. (13) can be simplified further as:

$$a_2 = \frac{1}{2} u K^{\text{hs}} \rho_s \frac{\partial a_1}{\partial \rho_s}, \quad (14)$$

where K^{hs} is the hard-sphere isothermal compressibility defined as:

$$K^{\text{hs}} = kT \left(\frac{\partial \rho_s}{\partial P^{\text{hs}}} \right)_T. \quad (15)$$

The SW radial distribution function at contact, needed in Eq. (5), is also calculated using the Barker–Henderson perturbation theory of the first order. A linear expansion of $g(r)$ gives:

$$g^{\text{SW}}(\sigma) = g^{\text{hs}}(\sigma) + \beta u g_1(\sigma), \quad (16)$$

and a logarithmic expansion of $g(r)$ [17] gives:

$$g^{\text{SW}}(\sigma) = g^{\text{hs}}(\sigma) \exp \left[\frac{1}{T^*} \frac{g_1(\sigma)}{g^{\text{hs}}(\sigma)} \right], \quad (17)$$

where $g^{\text{hs}}(\sigma)$ is the Carnahan–Starling hard-sphere radial distribution function at contact, given in [18], and $g_1(\sigma)$ is the perturbation term given in [19]:

$$g_1(\sigma) = \frac{1}{4u} \frac{\partial a_1}{\partial \eta} + \lambda^3 g^{\text{hs}}(\lambda\sigma), \quad (18)$$

or [14]:

$$g_1(\sigma) = \frac{1}{4u} \left[\frac{\partial a_1}{\partial \eta} - \frac{\lambda}{3\eta} \frac{\partial a_1}{\partial \lambda} \right], \quad (19)$$

where η is the reduced density defined as:

$$\eta = \frac{\pi}{6} \sigma^3 \rho_s^*. \quad (20)$$

4. Approaches to estimating a_1 , a_2 and $g^{\text{SW}}(\sigma)$

4.1. Empirical approach

For SW fluids, with $\lambda = 1.5$, Barker–Henderson [11] correlated their MC data for a_1 and a_2 as follows:

$$a_1 = uC_1 \left[1 - \exp\left(-\frac{\alpha_1 \rho^*}{\beta_1 - \rho^*}\right) - \frac{\alpha_1}{\beta_1} \rho^* \right] + p_1 \rho^* + q_1 (\rho^*)^2, \quad (21)$$

$$a_2 = u^2 C_2 \left[1 - \exp\left(-\frac{\alpha_2 \rho^*}{\beta_2 - \rho^*}\right) - \frac{\alpha_2}{\beta_2} \rho^* \right] + p_2 \rho^* + q_2 (\rho^*)^2, \quad (22)$$

where ρ^* is the reduced number density defined as $\rho_s \sigma^3$. The constants of Eqs. (21) and (22) are listed in Table 1.

Chen and Kreglewski [20] proposed an alternative equation for the dispersion term:

$$\tilde{a}_o^{\text{disp}} = \sum_{i=1}^4 \sum_{j=1}^9 D_{ij} \left(\frac{u}{kT} \right)^i \left(\frac{\eta}{\tau} \right)^j, \quad (23)$$

where $\tau = 0.74048$ and D_{ij} s are universal constants derived, e.g., from fitting the argon data; such D_{ij} s are used in the SAFT equation of state developed by Huang and Radosz [6].

The radial distribution function of the reference at contact, $g^{\text{SW}}(\sigma)$, is obtained from Eqs. (16) and (18), where $g^{\text{hs}}(\lambda\sigma)$ is interpolated from fitting MC data [10]:

$$g^{\text{hs}}(1.5\sigma) = 1 + \gamma_1 \eta + \gamma_2 \eta^2 + \gamma_3 \eta^3 + \gamma_4 \eta^4, \quad (24)$$

where γ_1 , γ_2 , γ_3 , and γ_4 are numerical coefficients listed in Table 2.

Table 1
The constants for a_1 and a_2 in Eqs. (21) and (22)

	1	2
C	3.173136	-0.384466
α	4.5	9.75
β	$\sqrt{2}$	$\sqrt{2}$
p	-4.974192	-2.487096
q	5.134186	-0.047652

Table 2

The coefficients for $g^{\text{hs}}(1.5\sigma)$ in Eq. (24)

γ_1	0.653305
γ_2	-1.381460
γ_3	-7.588440
γ_4	8.401660

4.2. Analytical approach

Eq. (12) can also be solved analytically; the result is dependent on the expression of the hard-sphere radial distribution function used. For example, Chang and Sandler [21] proposed a real-function expression for g^{hs} using the Percus–Yevick (PY) approximation. Their expression for the first shell, i.e., $\sigma < r < 2\sigma$, is as follows:

$$g^{\text{hs}}(x, \eta) = \frac{1}{x} [k_1 \exp\{A(x-1)\} + k_2 \exp\{B(x-1)\} \cos\{C(x-1)\} + k_3 \exp\{B(x-1)\} \sin\{C(x-1)\}], \quad (25)$$

where the expressions of k_i , A , B and C , are given in Ref. [21] and x is the reduced distance between two segments, r/σ . For $1 < \lambda < 2$, Chang and Sandler [12] solved Eqs. (12) and (14) to get:

$$a_1 = -12u\eta I, \quad (26)$$

$$a_2 = -6u^2\eta \frac{(1-\eta)^4}{1+4\eta+4\eta^2} \left[I + \eta \frac{\partial I}{\partial \eta} \right], \quad (27)$$

with:

$$I = \int_1^\lambda g^{\text{hs}}(x) x^2 dx = \sum_{n=1}^3 k_n t_n, \quad (28)$$

where the expressions of t_n are given in Ref. [21]. In Eq. (27), the PY approximation for the hard-sphere compressibility has been used.

Another approach to solving Eq. (12) on the basis of a mean-value theorem has been proposed by Gil-Villegas et al. [14]; they solved the integral using the mean value of the hard-sphere radial distribution function, $g^{\text{hs}}(\xi)$. Instead of using the mean value of distance ξ in the hard-sphere radial distribution function directly, they used the contact value but evaluated at an effective reduced density η_{eff} . This way, the result is much simpler, even though a parameterization is still needed to make the equations tractable. Their final expression for a_1 is as follows:

$$a_1 = -4\eta u (\lambda^3 - 1) g^{\text{hs}}(\sigma, \eta_{\text{eff}}), \quad (29)$$

where η_{eff} is related to the real reduced density η by a polynomial parameterization:

$$\eta_{\text{eff}} = c_1\eta + c_2\eta^2 + c_3\eta^3, \quad (30)$$

and c_1 , c_2 and c_3 are the polynomial coefficients. For $1.1 \leq \lambda \leq 1.8$, the coefficients have been obtained as functions of λ using exact values of a_1 obtained by integrating Eq. (12). Accurate values of $g^{\text{hs}}(r)$ calculated by solving the Ornstein–Zernike equation with Malijevsky and Labik formula have been used for this purpose.

The radial distribution function of the reference at contact, $g^{\text{SW}}(\sigma)$, is obtained from Eq. (16) or Eq. (17) and Eq. (18) or Eq. (19).

5. Dimer SW reference

The Helmholtz energy contribution due to bond formation, \tilde{a}^{chain} , given by Eq. (5), is for a monomer reference TPT1. This contribution is equivalent to the change of the Helmholtz energy upon dimerization at constant temperature and monomer density [13]. Each bond in a chain is considered to be a dimer bond, and the interdependence of bonds is neglected.

This approach can be extended to a dimer reference TPT1 (TPT1-D) that incorporates the structural information on the SW-dimer fluid [13]. The chain formation is assumed to occur in two steps. The first step is the formation of dimers from monomers, as in TPT1. The second step is the formation of chains from dimers; hence, dimers become the reference. The cumulative effect of bonding in the second step is estimated by multiplying the contribution due to forming one tetramer from dimers by the number of bonds required to form a chain of dimers.

The overall Helmholtz energy due to bond formation in TPT1-D, which supersedes Eq. (5) in TPT1, is therefore calculated as follows:

$$\begin{aligned} \tilde{a}^{\text{chain}} = & -\frac{m}{2} [\ln g^{\text{SW-mono}}(\sigma) - \ln g_0^{\text{SW-mono}}(\sigma)] \\ & -\frac{m-2}{2} [\ln g^{\text{SW-dimer}}(\sigma) - \ln g_0^{\text{SW-dimer}}(\sigma)], \end{aligned} \quad (31)$$

where $g^{\text{SW-mono}}$ is the correlation function for SW monomers and $g^{\text{SW-dimer}}$ is the site–site angle-averaged correlation function for SW dimer. The first term on the right side of Eq. (31) is the energy contribution of the dimer bond formation (first step) and the second term on the right side of Eq. (31) is the energy contribution of the chain formation (second step). Eq. (31) can also be written as:

$$\begin{aligned} \tilde{a}^{\text{chain}} = & -(m-1) [\ln g^{\text{SW-mono}}(\sigma) - \ln g_0^{\text{SW-mono}}(\sigma)] \\ & -\frac{m-2}{2} [\ln g^{\text{SW-corr}}(\sigma) - \ln g_0^{\text{SW-corr}}(\sigma)], \end{aligned} \quad (32)$$

where $g^{\text{SW-corr}}$ is defined as:

$$g^{\text{SW-corr}}(\sigma) = \frac{g^{\text{SW-dimer}}(\sigma)}{g^{\text{SW-mono}}(\sigma)}. \quad (33)$$

Correlation for $g^{\text{SW-corr}}$ has been developed [13] using MC simulation data:

$$g^{\text{SW-corr}}(\sigma) = \alpha_0(T^*) + \alpha_1(T^*)\rho^* + \alpha_2(T^*)(\rho^*)^2 + \alpha_3(T^*)(\rho^*)^3 + \alpha_4(T^*)(\rho^*)^4, \quad (34)$$

where α_i s are temperature-dependent parameters given in Ref. [13].

6. SW SAFT models studied

We select six SW SAFT models for real fluids, numbered 1 through 6, by combining the different approaches discussed above. These models are defined in Table 3. For all models, as proposed in Ref. [22], we use a temperature-dependent potential-well depth u to account for the non-central forces:

$$u = u^o \left(1 + \frac{e}{kT} \right), \quad (35)$$

where u^o is the temperature-independent potential-well depth and e/k is a constant (methane: $e/k = 1$, other n -alkanes: $e/k = 10$). In all models, the radial distribution function is calculated using the linear expansion of $g(r)$, Eq. (16), and $g_1(\sigma)$ is calculated using Eq. (18) or Eq. (19). The expression of a_1 used in Eq. (18) or Eq. (19) is consistent with that in the dispersion term.

Model 1 is an empirical SW SAFT model. MC fit is used to calculate the dispersion term of the Helmholtz energy and $g^{\text{hs}}(\lambda\sigma)$. As in Ref. [23], the segment diameter is temperature-dependent, defined as:

$$d = \int_0^\sigma [1 - \exp(-\beta\phi(r))] dr. \quad (36)$$

To integrate Eq. (36), we apply the inverted SW model proposed by Kreglewski [23] and obtain:

$$d = \sigma \left[1 - 0.12 \exp\left(-\frac{3u^o}{kT}\right) \right]. \quad (37)$$

Thus, in this model, the reduced density η and the reduced number density ρ^* are defined in terms of the effective segment diameter d , instead of σ .

Table 3
The SW SAFT models studied

Model	Dispersion term	Chain term	$g^{\text{hs}}(\lambda\sigma)$ in Eq. (18)	λ	m
1	Barker–Henderson’s MC fit, Eqs. (21) and (22)	Monomer reference, Eq. (5)	Banaszak et al.’s MC fit, Eq. (24)	1.5	
2	Argon fit, Eq. (23)	Monomer reference, Eq. (5)	Banaszak et al.’s MC fit, Eq. (24)	1.5	
3	Analytic PY approximation, Eqs. (26) and (27)	Monomer reference, Eq. (5)	Banaszak et al.’s MC fit, Eq. (24)	1.5	
4	Mean value theorem, Eqs. (14) and (29)	Monomer reference, Eq. (5)	Mean value theorem, see Eq. (19)	1.5	
5	Mean value theorem, Eqs. (14) and (29)	Monomer reference, Eq. (5)	Mean value theorem, see Eq. (19)	vary	$1 + (n_c - 1)/3$
6	Argon fit, Eq. (23)	Dimer reference, Eq. (32)	Banaszak et al.’s MC fit, Eq. (24)	1.5	

Model 2 is also an empirical model. The dispersion term of the Helmholtz energy is the argon fit and the other equations are the same as that in model 1. This model is analogous to the Huang–Radosz [6] version of SAFT, except for g^{hs} .

Model 3 is a semi-analytical model that uses an analytical approach to calculate the dispersion term of the Helmholtz energy and an empirical approach to calculate $g^{\text{hs}}(\lambda\sigma)$. The reduced density η and the reduced number density ρ^* are defined in terms of the effective segment diameter d .

Models 4 and 5 are analytical models based on the approach developed by Gil–Villegas et al. [14]. With the use of the mean value theorem and PY approximation for K^{hs} , the dispersion term of the Helmholtz energy and the radial distribution function are calculated analytically. As in their work, the segment diameter is assumed to be independent of temperature, but the energy parameter is temperature-dependent according to Eq. (35). Also, in model 4, we fix the value of λ ($\lambda = 1.5$), whereas in model 5, we allow the value of λ to vary and use a simple correlation for m as a function of molecular weight or number of carbon.

In model 6, which is empirical, we examine the effect of the inclusion of SW dimer structural information in the chain term. Based on model 2, we replace Eq. (5) with the dimer reference chain term, Eq. (32), and apply the MC fit, Eq. (34), to calculate $g^{\text{SW-corr}}(\sigma)$.

7. Results and discussion

Before applying the models described above, we analyze the underlying approximations, and illustrate their performance. Fig. 2 illustrates behavior of the first perturbation term \tilde{a}_1 as a function of reduced number density for models 1, 3, and 4 (or 5) calculated for $\lambda = 1.5$. It turns out that the curves calculated from the empirical and analytical models nearly coincide.

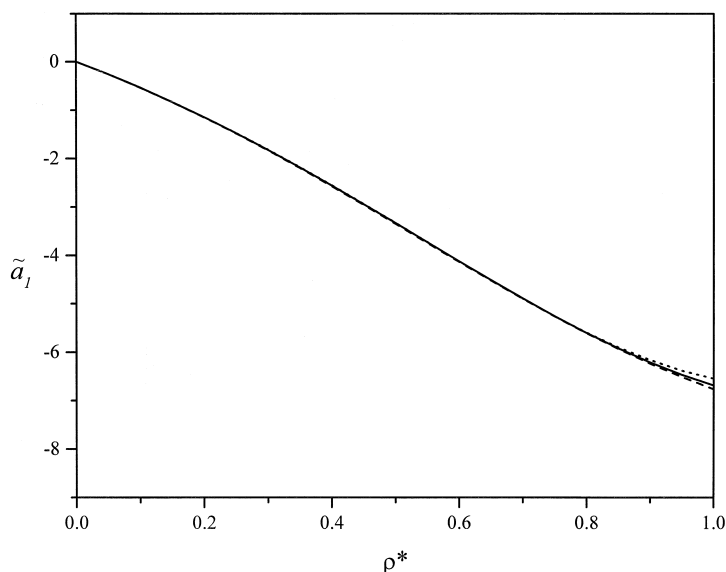


Fig. 2. The dimensionless first-order perturbation term \tilde{a}_1 for $\lambda = 1.5$ as a function of reduced number density ρ^* (dashed curve: model 1, dotted curve: model 3, solid curve: model 4 or 5).

Fig. 3 illustrates the behavior of the second perturbation term \tilde{a}_2 for models 1, 3, and 4 (or 5) also calculated for $\lambda = 1.5$. We note that \tilde{a}_2 calculated from the local compressibility approximation, in models 3 and 4, does not agree with the simulation results. Besides the Barker–Henderson simulation result, which is model 1, we also show the simulation result of Alder et al. [24].

Fig. 4 illustrates the dispersion term per segment $\tilde{a}_0^{\text{disp}}$ for models 1, 2, 3, and 4 (or 5) with $\lambda = 1.5$ and at $T^* = 0.75$. At this particular reduced temperature, models 1, 3, and 4 result in similar values of $\tilde{a}_0^{\text{disp}}$, except in the high-density range. Although \tilde{a}_2 of model 1 is very different from those of models 3 and 4, its contribution to $\tilde{a}_0^{\text{disp}}$ is not large. However, we may expect that the contribution of \tilde{a}_2 to the dispersion term will be larger at lower reduced temperatures. It is also interesting to note that the argon fit shown in Fig. 4, which is model 2, has a much lower absolute value of the dispersion term than those of the other models.

Fig. 5 illustrates the radial distribution function at contact for model 1 (or 2), 3, and 4 (or 5) at $\lambda = 1.5$, $T^* = 0.75$, and for hard-sphere fluid with CS approximation. The points are the MC simulation data [25]. At this particular temperature, the radial distribution function calculated from all the models except CS are lower than those obtained from the MC simulation for $\rho^* < 0.8$. This figure also suggests that all the models imply a similar radial distribution function, except in high-density range ($\rho^* > 0.8$).

Fig. 6 illustrates the chain contribution to the Helmholtz energy due to one bond formation, \tilde{a}^{bond} , for models 1 (or 2), 3, and 4 (or 5) with $\lambda = 1.5$ and at $T^* = 0.75$. We find that all these models imply similar estimates of \tilde{a}^{bond} .

Next, we fit all the models to experimental saturated-vapor pressure and saturated-liquid volume data for *n*-alkanes over the same temperature range as in Ref. [6]. In our optimization procedure, we

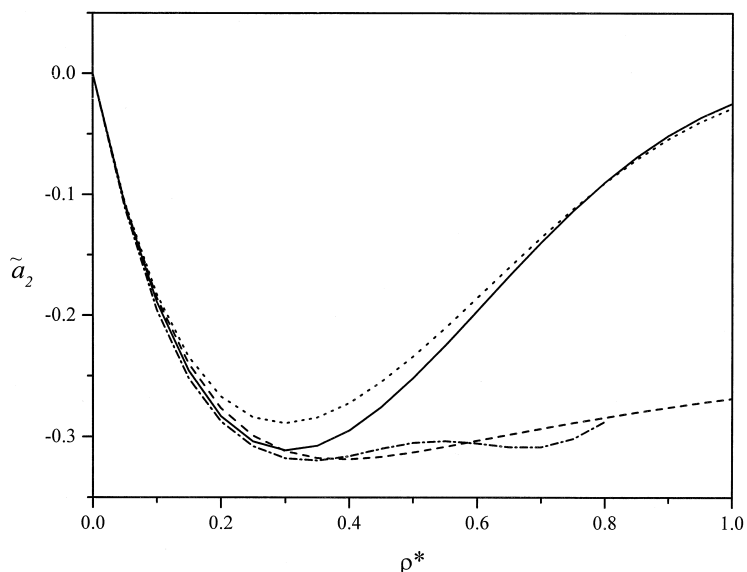


Fig. 3. The dimensionless second-order perturbation term \tilde{a}_2 for $\lambda = 1.5$ as a function of reduced number density ρ^* (dashed curve: model 1, dotted curve: model 3, solid curve: model 4 or 5). The dotted–dashed curve is a smoothed curve of the simulation results of Alder et al. [24].

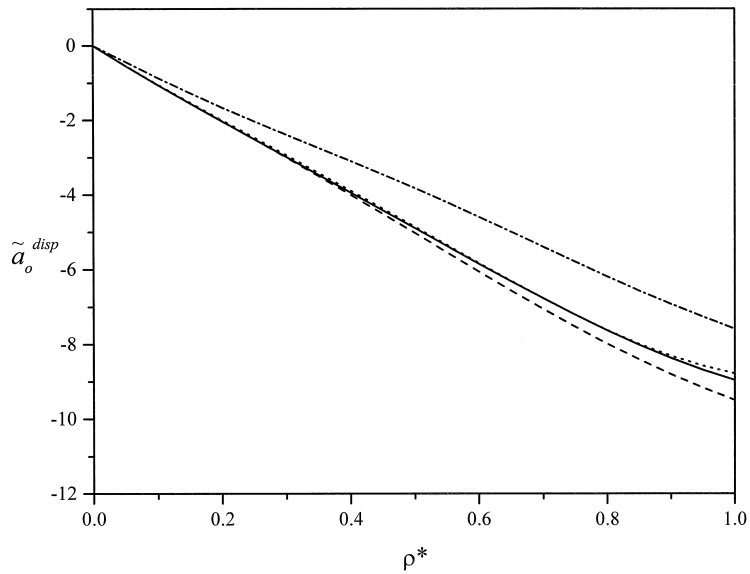


Fig. 4. The dispersion term per segment for $\lambda = 1.5$ at $T^* = 0.75$ as a function of reduced number density ρ^* (dashed curve: model 1, dotted–dashed curve: model 2, dotted curve: model 3, solid curve: model 4 or 5).

give an equal weight to both properties. The results are presented in Table 4. The average values of average absolute deviation (AAD) for the liquid volume and the vapor pressure are also shown in Table 4.

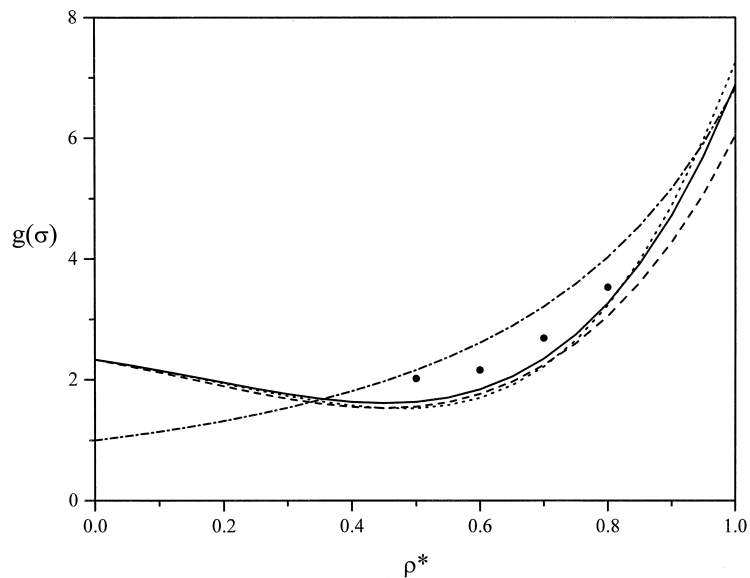


Fig. 5. Values of $g(\sigma)$ for hard-sphere fluid with CS (dotted–dashed curve) approximation and for the SW fluid with $\lambda = 1.5$ at $T^* = 0.75$ (dashed curve: model 1 or 2, dotted curve: model 3, solid curve: model 4 or 5). The points are the MC data of Henderson et al. [25].

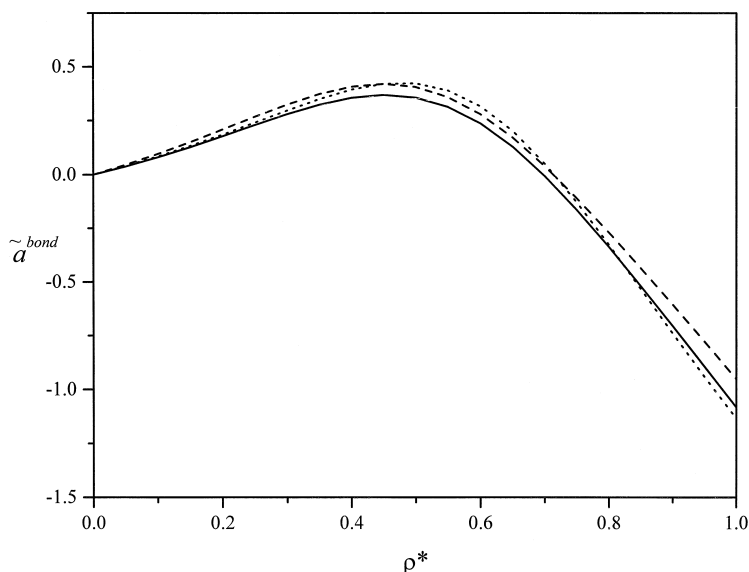


Fig. 6. The chain contribution to the Helmholtz energy as a function of reduced number density ρ^* (dashed curve: model 1 or 2, dotted curve: model 3, solid curve: model 4 or 5), $\lambda = 1.5$, $T^* = 0.75$.

For all SW SAFT models, the segment diameter σ (or segment volume v^{oo}) and the segment energy u^o/k increase with increasing molecular weight, as shown in Figs. 7 and 8. The segment volume is related to the segment diameter by the following equation:

$$v^{oo} = \frac{\pi N_{Av}}{6\tau} \sigma^3, \quad (38)$$

where N_{Av} is the Avogadro number.

Model 1 agrees with MC data [10], but it does not correlate the liquid volume well when it is applied to the real fluids, as shown in Table 4. As shown in Figs. 7 and 8, model 1 also has large and variable values of the segment volume (v^{oo}) and segment energy (u^o/k) for long chains. This feature is undesirable for mixtures having large differences in molar mass (the difference in segment parameters becomes large). Fig. 9 illustrates this problem for a mixture of ethane and *n*-decane (dashed curve represents model 1).

Model 2 exhibits a better goodness of fit for the vapor pressure, as shown in Table 4. This is probably due to the fact that the universal constants of Eq. (23) are obtained from data for a real substance, i.e., argon. Model 2 also gives lower values of the segment volume and energy for long chains, compared to model 1; the payoff (dotted curve) is shown in Fig. 9. Let us note that model 2 is similar to the Huang–Radosz [6] SAFT equation of state, except for the SW radial distribution function in the chain term, here used in place of the hard-sphere radial distribution function. Figs. 10 and 11 show the effect of this difference; using the SW radial distribution function amounts to accounting for the attractive energy in determining the energy of bond formation. The examples in Figs. 10 and 11 are for the coexisting vapor and liquid density of propane. Model 2 seems to improve slightly the representation of the vapor density, but there is little difference in the liquid density and critical region.

Table 4

The model parameters for *n*-alkanes

	1				2				3			
	<i>m</i>	v^{oo} [cm ³ /mol]	u^o/k [K]	AAD % <i>P/V</i>	<i>m</i>	v^{oo} [cm ³ /mol]	u^o/k [K]	AAD % <i>P/V</i>	<i>m</i>	v^{oo} [cm ³ /mol]	u^o/k [K]	AAD % <i>P/V</i>
Methane	0.900	23.493	141.38	0.76/1.8	0.991	21.673	190.97	0.1/0.13	1.041	19.754	156.00	0.94/2.2
Ethane	1.054	29.582	239.71	1.1/3.6	1.168	27.551	278.10	0.45/2.1	1.196	25.198	265.37	1.3/2.6
Propane	1.208	35.116	317.14	0.75/4.0	1.426	30.987	311.26	0.62/3.6	1.343	30.446	350.96	1.8/2.0
Butane	1.333	40.600	390.07	1.1/5.2	1.673	33.735	335.98	1.2/5.1	1.428	36.662	425.68	2.0/2.2
Pentane	1.434	44.881	457.71	0.62/2.9	1.921	34.780	354.17	0.67/3.5	1.560	40.040	506.36	2.8/1.4
Hexane	1.543	49.597	523.35	1.6/3.9	2.182	36.147	365.55	1.4/4.5	1.612	44.629	569.15	4.7/3.2
Heptane	1.635	54.212	584.44	2.2/4.1	2.430	37.351	375.20	1.7/4.6	1.632	53.313	617.87	7.9/2.5
Octane	1.721	58.366	643.13	2.4/3.5	2.674	38.171	383.20	1.5/3.9	1.715	57.527	681.19	7.2/2.4
Nonane	1.861	59.656	713.39	1.8/2.2	2.999	37.137	385.14	1.2/2.5	1.862	57.653	762.85	7.6/3.7
Decane	1.927	64.742	766.57	2.9/3.4	3.282	37.814	388.28	1.5/3.4	1.883	66.901	803.54	11.3/3.5
Average				1.5/3.5				1.0/3.3				4.8/2.6
	4				5				6			
	<i>m</i>	v^{oo} [cm ³ /mol]	u^o/k [K]	AAD % <i>P/V</i>	v^{oo} [cm ³ /mol]	u^o/k [K]	λ	AAD % <i>P/V</i>	<i>m</i>	v^{oo} [cm ³ /mol]	u^o/k [K]	AAD % <i>P/V</i>
Methane	1.051	19.307	149.191	0.49/1.0	20.795	161.972	1.465	0.26/1.2	1.374	15.708	156.76	0.83/2.3
Ethane	1.244	24.101	216.635	0.68/2.4	21.916	195.317	1.541	0.70/2.2	1.506	21.261	239.20	1.0/3.7
Propane	1.478	27.662	245.941	0.66/2.8	23.324	201.794	1.581	0.28/2.4	1.667	26.304	284.07	0.82/4.2
Butane	1.689	30.764	269.227	1.1/3.9	24.343	208.016	1.600	1.0/3.4	1.809	31.144	320.99	1.2/5.5
Pentane	1.885	32.734	287.766	0.80/1.9	24.390	206.570	1.630	0.43/1.3	1.947	34.320	351.18	0.70/3.5
Hexane	2.125	34.227	298.026	1.5/2.8	24.910	208.234	1.641	0.73/1.9	2.097	38.188	373.25	1.5/4.9
Heptane	2.329	35.870	308.290	1.5/2.9	25.156	207.699	1.654	0.68/2.0	2.264	40.556	390.91	1.7/4.7
Octane	2.532	37.110	316.639	1.3/2.3	25.209	206.054	1.668	0.55/1.3	2.403	43.141	407.36	1.4/4.0
Nonane	2.806	36.850	319.816	1.4/1.3	25.363	208.695	1.668	0.88/0.51	2.593	43.876	418.44	1.1/2.6
Decane	3.046	37.593	323.761	1.5/1.8	25.609	211.645	1.665	0.95/0.84	2.792	45.846	426.01	1.3/3.8
Average				1.1/2.3				0.65/1.7				1.2/3.9

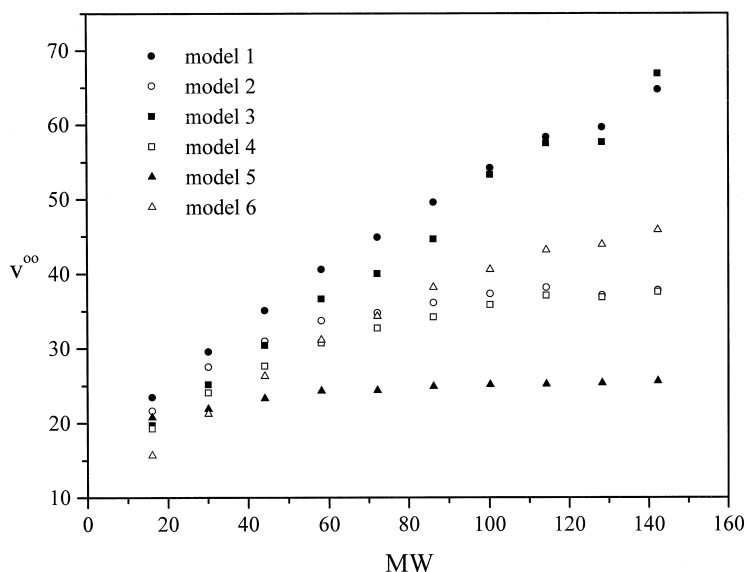


Fig. 7. The segment volume parameters for *n*-alkanes as a function of molecular weight.

Model 3 does not fit the vapor pressure and liquid volume well, as shown in Table 4. It also has the same problem as model 1, i.e., it gives large values of the segment volume and energy for long chains. Recently, Tavares et al. [26] developed a completely analytic model. Their model, with temperature-independent parameters, is the same as model 3, except that instead of applying the empirical Eq. (24), they applied Eq. (25) to calculate $g^{hs}(\lambda\sigma)$ and used a logarithmic expansion

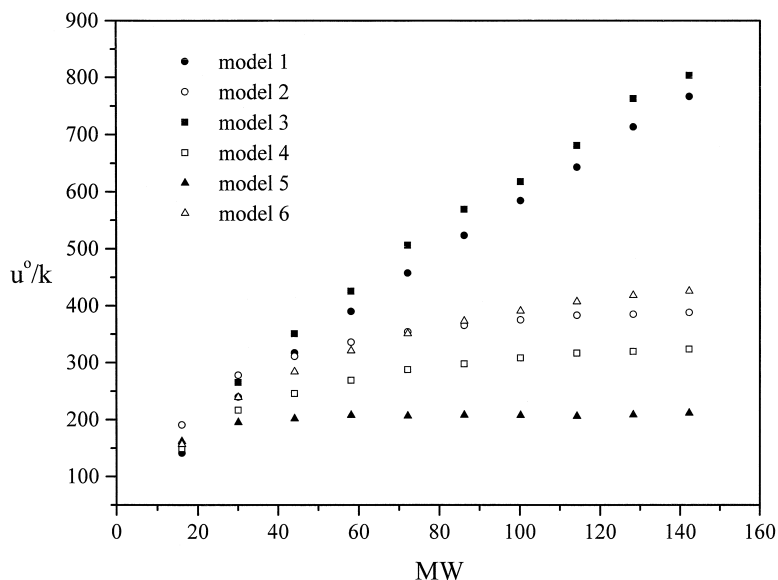


Fig. 8. The segment energy parameters for *n*-alkanes as a function of molecular weight.

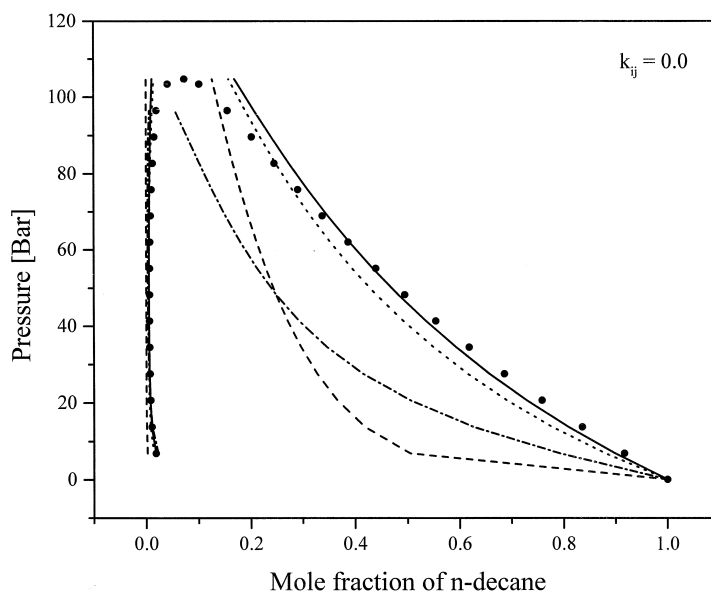


Fig. 9. Vapor–liquid equilibria in ethane + *n*-decane at 378 K, experimental [27] (points) and predicted (dashed curve: model 1, dotted curve: model 2, solid curve: model 5, dotted–dashed curve: model 6).

Eq. (17) to calculate $g(r)$. Eq. (17) gives the exact limit at zero density, $\exp(1/T^*)$, whereas Eq. (16) gives an approximate limit, $1 + (1/T^*)$. That model, with variable λ , was shown to fit the experimental vapor pressure and critical point data well. We instead fit it to experimental saturated-

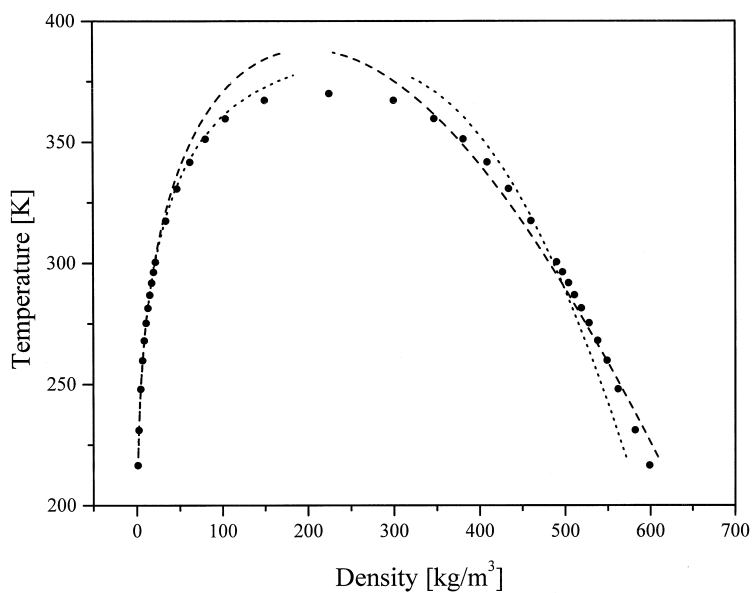


Fig. 10. Coexisting vapor and liquid density of propane, experimental [28] (points) and calculated (dashed curve: SAFT, dotted curve: model 2).

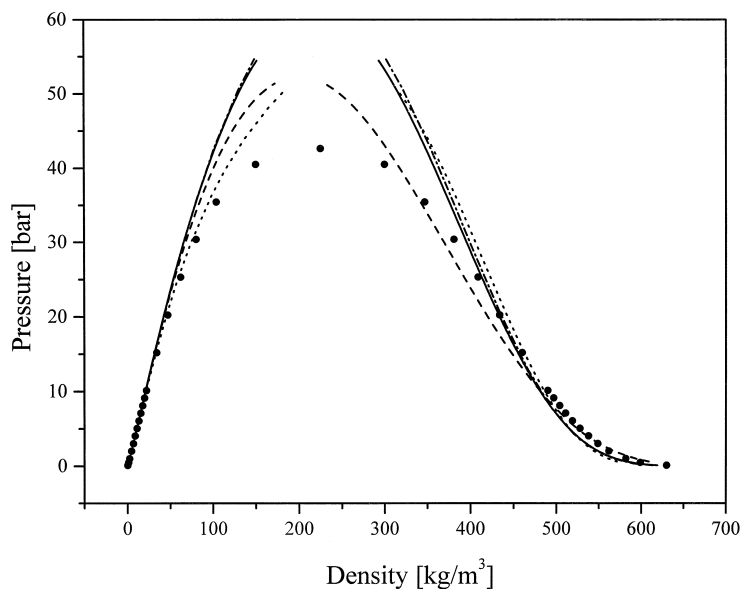


Fig. 11. Coexisting vapor and liquid density for propane, experimental [28] (points) and calculated (dashed curve: SAFT, dotted curve: model 2, dotted–dashed curve: model 4, solid curve: model 5).

vapor pressure and saturated-liquid volume, and find that there is a problem with representing the saturated-liquid volume. This is probably due to the use of the PY approximation in calculating $g^{\text{hs}}(r)$ because the PY approximation does not give accurate values of the radial distribution function in the high-density range.

Models 4 and 5 seem to give a good combination of the accuracy for the vapor pressure and liquid volume, as shown in Table 4, of the parameter behavior, as shown in Figs. 7 and 8, and of the mixture phase behavior, as shown in Fig. 9. These models are similar to the SAFT equation of state in representing the liquid density and critical region, as shown in Figs. 11 and 12. In the pressure-density plane, as shown in Fig. 11, the coexisting curve is better represented by SAFT. To characterize the performance at low densities, the estimated second virial coefficient is shown in Fig. 13 for *n*-octane; model 5 overestimates the second virial coefficient even at high temperatures. The poor representation of the critical region and the second virial coefficient are probably due to the fact that the convergence of the Barker–Henderson perturbation theory is slow in the critical region and at low densities, and hence, the first two perturbation terms alone may not be adequate.

Model 6 gives higher values of the segment parameters than those of model 2, as shown in Figs. 7 and 8, which results in poor predictions for mixtures, as shown in Fig. 9. Fig. 13 shows a small improvement gained from the dimer reference for the second virial coefficient (dotted–dashed curve). One reaches the same conclusion if one includes the dimer structure information in the hard-chain term in the SAFT equation of state.

Although the models considered here, except for model 2, represent almost the same Helmholtz energy, they significantly differ in representing real fluids. Models that result in high values of u°/k are less desirable because they cause lower values of T^* ($= T/(u/k)$) and, hence, slower convergence of the perturbation series. This probably makes Eq. (11) misrepresent the real systems. For

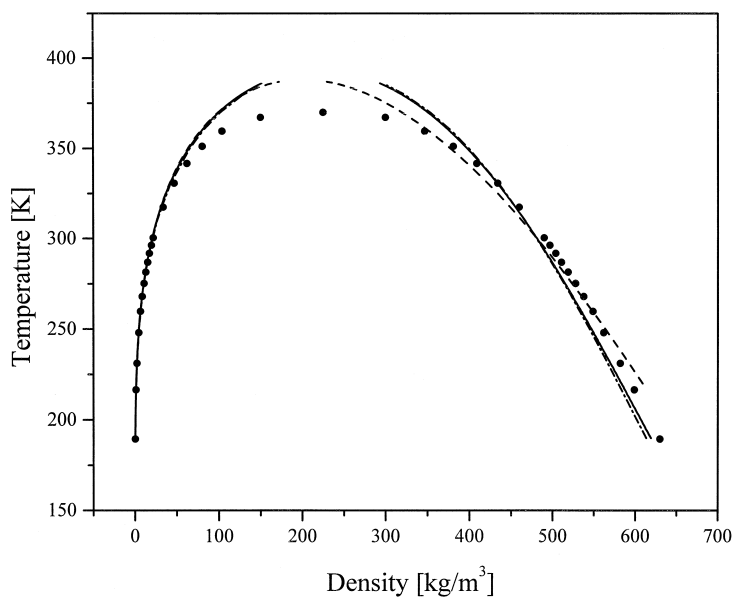


Fig. 12. Coexisting vapor and liquid density for propane, experimental [28] (points) and calculated (dashed curve: SAFT, dotted–dashed curve: model 4, solid curve: model 5).

example, a temperature of 303 K for *n*-octane corresponds to T^* of 0.46 for model 1, 0.43 for model 3, 0.93 for model 4, and 1.42 for model 5; the lower the T^* , the slower the convergence. Also, a strong molecular weight dependence of u^o/k and v^{oo} is undesirable because, as the mixture

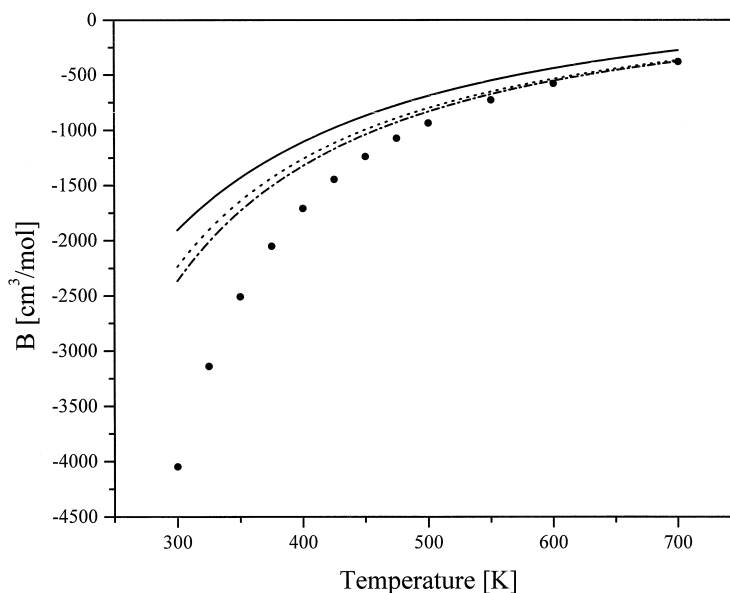


Fig. 13. Second virial coefficient of *n*-octane, experimental [29] (points) and predicted (dotted curve: model 2, solid curve: model 5, dotted–dashed curve: model 6).

components differ more and more in the values of their parameters, the mixing rules become less and less reliable.

8. Conclusion

Six SW SAFT models, fitted to the experimental saturated liquid volume and saturated vapor pressure for pure *n*-alkanes, are analyzed for predicting the coexisting densities, second virial coefficients, and binary phase equilibria. The models that result in low values of the segment energy and weak molecular weight dependence of the parameters are found to be more accurate for real fluids. For example, model 5 seems to provide a good basis for further development because it is based on an analytical approach, gives the lowest values of the segment energy and volume, and the smallest difference in the segment parameters between different molecules.

The inclusion of the dimer structure in the SW chain term seems to produce no significant benefit for representing real substances. This is probably because the contribution of bond formation to the total Helmholtz energy is relatively small.

9. List of symbols

a	molar Helmholtz free energy
a_1, a_2	the first and second perturbation terms of Helmholtz free energy, associated with the attractive energy u
d	the temperature-dependent segment diameter
D_{ij}	universal constants used in Eq. (23)
g	the radial distribution function
g_1	the first perturbation term of g^{SW}
I	integral defined in Eq. (28)
k	the Boltzmann constant
K	isothermal compressibility
m	the number of segments per molecule
N_{Av}	the Avogadro number
P	pressure
r	molecular distance
R	gas constant
T	temperature
T^*	dimensionless temperature
u	the temperature-dependent well depth of the SW potential
u°	the temperature-independent well depth of the SW potential
$v^{\circ\circ}$	the segment molar volume
x	the reduced distance between two segments, r/σ .
<i>Greek</i>	
β	$1/kT$
ϕ	the intermolecular potential

ϕ_1	the perturbation potential
η	reduced density
λ	the reduced potential well range
ρ	molar density
ρ_s	number density
ρ^*	reduced number density
σ	the temperature-independent segment diameter

Superscripts

assoc	association
disp	dispersion
hs	hard sphere
res	constant-volume residual
seg	segment
SW	square well
~	dimensionless

Subscripts

0	calculated at zero density
eff	effective
o	per segment

Acknowledgements

The funding for this work was provided in part by the U.S. Department of Energy as Grant No. DE-FG02-96ER12201.

References

- [1] M.S. Wertheim, J. Stat. Phys. 35 (1984) 19.
- [2] M.S. Wertheim, J. Stat. Phys. 35 (1984) 35.
- [3] M.S. Wertheim, J. Stat. Phys. 42 (1986) 459.
- [4] M.S. Wertheim, J. Stat. Phys. 42 (1986) 477.
- [5] W.G. Chapman, K.E. Gubbins, G. Jackson, M. Radosz, Fluid Phase Equilib. 52 (1989) 31.
- [6] S.H. Huang, M. Radosz, Ind. Eng. Chem. Res. 29 (1990) 2284.
- [7] M. Banaszak, C.K. Chen, M. Radosz, Macromolecules 29 (1996) 6481.
- [8] M. Banaszak, Y.C. Chiew, R. O'Lenick, M. Radosz, J. Chem. Phys. 100 (1994) 3803.
- [9] M. Banaszak, Y.C. Chiew, M. Radosz, Fluid Phase Equilib. 111 (1995) 161.
- [10] M. Banaszak, Y.C. Chiew, M. Radosz, Phys. Rev. E 48 (1993) 3760.
- [11] J.A. Barker, D. Henderson, Annu. Rev. Phys. Chem. 23 (1972) 439.
- [12] J. Chang, S.I. Sandler, Mol. Phys. 81 (1994) 745.
- [13] F.W. Tavares, J. Chang, S.I. Sandler, Mol. Phys. 86 (1995) 1451.
- [14] A. Gil-Villegas, A. Galindo, P.J. Whitehead, S.J. Mills, G. Jackson, J. Chem. Phys. 106 (1997) 4168.
- [15] D.A. McQuarrie, Statistical Mechanics, Harper Collins Publisher, New York, 1976.
- [16] N.F. Carnahan, K.E. Starling, J. Chem. Phys. 51 (1969) 635.
- [17] J.A. Barker, D. Henderson, Review of Modern Physics 48 (1976) 587.

- [18] T.M. Reed, K.E. Gubbins, *Applied Statistical Mechanics*, McGraw-Hill, New York, 1973.
- [19] D. Henderson, J.A. Barker, W.R. Smith, *J. Chem. Phys.* 64 (1976) 4244.
- [20] S.S. Chen, A. Kreglewski, *Ber. Bunsen-Ges. Phys. Chem.* 81 (1977) 1048.
- [21] J. Chang, S.I. Sandler, *Mol. Phys.* 81 (1994) 735.
- [22] A. Kreglewski, R.C. Wilhoit, *J. Phys. Chem.* 78 (1974) 1961.
- [23] A. Kreglewski, *Equilibrium Properties of Fluids and Fluid Mixtures*, Texas A&M University Press, 1984.
- [24] B.J. Alder, D.A. Young, M.A. Mark, *J. Chem. Phys.* 56 (1972) 3013.
- [25] D. Henderson, W.G. Madden, D.D. Fitts, *J. Chem. Phys.* 64 (1976) 5026.
- [26] F.W. Tavares, J. Chang, S.I. Sandler, *Fluid Phase Equilib.* 140 (1997) 129.
- [27] H.H. Reamer, B.H. Sage, *J. Chem. Eng. Data* 7 (1962) 161.
- [28] N.B. Vargaftik, *Tables on the Thermophysical Properties of Liquids and Gases*, Wiley, New York, 1975.
- [29] J.H. Dymond, E.B. Smith, *The Virial Coefficients of Pure Gases and Mixtures*, Oxford Univ. Press, New York, 1980.